*Materials Characterization,* 73 (2012) 16-30
DOI:http://dx.doi.org/10.1016/j.matchar.2012.06.013

# Serrated flow in powder metallurgy Al–5%Mg–1.2%Cr alloy processed by equal channel angular pressing

*M. Eddahbi**, *M.A. Monge*, *A. Muñoz*, *R. Pareja*

*Departamento de Física, Universidad Carlos III de Madrid, 28911 Leganés, Madrid, Spain*

**Abstract:** The microstructure, texture and mechanical behavior of the powder metallurgy Al 5 w t . % M g 1.2 wt.%Cr alloy subjected to equal channel angular pressing (ECAP) has been investigated. The material processed by ECAP, as well as in the homogenized condition, exhibited room temperature serrated flow (SF) up to fracture. The critical stress for the serration onset decreased with increasing strain rate or ECAP temperature. The results indicated that this SF was induced by shear banding. The stress oscillations were attributed to the interaction between shear bands (SBs) and obstacles like second phase particles, and dislocation locks produced by strain hardening. The early stages of the stress strain $\sigma$ $\varepsilon$ curves of the ECAP processed samples showed a transition from type B serrations with continuous strain hardening to type B serrations superimposed on a succession of constant stress plateaus when the tensile strain rate was increased from $10^{-4}s^{-1}$ to $10^{-3}s^{-1}$. The plateaus in $\sigma$ $\varepsilon$ curves obtained at a strain rate of $10^{-3}s^{-1}$ were ascribed to the nucleation of a band at one end of the sample gauge region and subsequent propagation towards the opposite end. At a low strain rate of $10^{-4}s^{-1}$ the sites for band nucleation should be randomly distributed along the sample gauge region. The disappearance of the plateaus in the $\sigma$ $\varepsilon$ curves are attributed to the activation of a new moving band before the completion of the deformation banding cycle of the preceding band.

**Keywords:** Aluminum alloys ECAP, Serrated flow Mechanical properties Shear banding

## 1. Introduction

Serrated flow (SF), or the Portevin Le Chatelier (PLC) effect, has been reported in several materials such as Fe, Ni, Cu and Al base alloys tested under different conditions [1 9]. This effect is a manifestation of discontinuous plastic flow, or plastic instabilities, from microstructural origin inducing either zero or negative strain rate sensitivity [10]. It is widely recognized that the interaction of solute atoms with mobile dislocations, i.e. dynamic strain aging (DSA), is the main source of SF [11,12]. Several types of serrations, labeled as types A trough D have been identified and their characteris tics reported [12]. These serration types, which depend on the test conditions and the state of the material, are found associated to the formation and propagation of localized deformation bands. Type A serrations are associated with the periodic nucleation of deformation bands at one of the ends of the tensile sample, and their continuous propagation toward the other end along the gauge region of the sample; this kind of serration occurs at low temperatures or high strain rates. Type B serrations are also associated with bands nucleated at one end but propagate discontinuously to the other end; they are characterized by a rapid succession of rather regular stress oscillations that arise from DSA of the mobile dislocations in the band. This serration type may be the result of a transformation of type A serrations into type B with increasing strain, or occurs at the onset of the SF for low strain rates and high deformation temperatures. Type C serrations are differentiated by regular saw tooth like stress drops with a rather high frequency below the track of the flow

* *Corresponding author:* Tel.: +34 91 624 8734; fax: +34 91 624 8749.
E mail address: meddahbi@fis.uc3m.es (M. Eddahbi).

curve; they are attributed to dislocation unlocking and occur at higher temperatures and lower strain rates than the other two serration types. The serrations consisting in a succession of stress plateaus in the stress strain curve, referred to as Type D, are attributed to propagation of bands without strain hardening. Type B serrations are often found superposed to type A or type D serrations.

Also, it has been found that the SF onset in substitutional alloys appears after attaining a threshold or critical strain, $\varepsilon_c$, which may depend on temperature, strain rate, grain size and solute content [6,11,13,14]. Furthermore, the initial amount of cumulative deformation and the strain path have an effect on the SF characteristics [8,15]. Although the effect of the severe plastic deformation on the SF character istics of the pure metals and alloys has been scarcely investigated, the PLC effect has been reported in Al Mg and Al Cu alloys processed by equal channel angular pressing (ECAP) [16 20]. Some of these results indicate that the submicron structures developed in Al Mg alloys by the ECAP processing exhibit less susceptibility to the PLC effect, and higher strain rate sensitivity, than the coarser ones [17 19]. However, other results suggesting the opposite has also been reported [16].

On the other hand, there exist models attributing the stress drops in the SF to the passage of the shear bands (SBs) through the grains [4]. Moreover, the SF behavior in some Al alloys has in part attributed to shearing of precipitates by dislocations and other precipitation effects [21 25]. I n particular, the precipitation treated samples deformed at a given strain rate exhibited lower critical strains and higher stress oscillations in comparison with the alloys in the as cast condition [22]. However, it should be noted that there are reports indicating that shearing of precipitates is not a sufficient requisite for the appearance of SF in Al alloys [26].

Al Mg alloys, which exhibit SF and poor creep resistance, might be suitable for automotive and aerospace applications if their formability is enhanced by preventing SF and improving the mechanical properties at elevated tempera tures. The SF inhibition would avoid the development of the detrimental localization of plastic flow in the parts during their forming processes. The enhancement of the creep resistance would allow fabricating drive train parts for operating temperatures above 120 °C. The addition of tran sition metals such as Cr or Fe enhances the microstructure stability and mechanical properties of the Al Mg alloys at elevated temperature via dispersion strengthening [27 29]. Among these alloys, rapidly solidified Al 5Mg 1.2Cr (wt.%) consolidated by extrusion is an attractive material for superplastic forming since it exhibits superplastic behavior at strain rate as high as $10^{-2}\,s^{-1}$ [30]. Although the processing effects on the microstructure of this alloy have been reported, its plastic flow characteristics are still little known [31].

The main objective of the present work was to investigate the effect of the ECAP processing on the Al 5Mg 1.2Cr alloy. In particular, an attempt has been made to describe the characteristics of the SF observed in stress strain ($\sigma$ $\varepsilon$) curves during room temperature (RT) deformation at strain rates of $10^{-4}s^{-1}$ and $10^{-3}s^{-1}$.

## 2. Experimental Procedure

The Al 5%Mg 1.2%Cr (wt.%) alloy was produced by sintering of rapidly solidified powder followed by extrusion. The details of the production and composition of the alloy are given in Ref. [31]. After a homogenization treatment at 500 °C for 48 h followed by furnace cooling, 10 mm×10 mm×50 mm billets were ECAP processed at 200 °C, 250 °C and 300 °C applying a pressing rate of 20 mm $min^{-1}$. The ECAP die had an internal angle of $\Phi$ 90° and an outer angle of $\Psi$ 0°, which produced an effective strain of ~1 by pass. The billets were subjected to a single pass, and two passes via routes B (2pB) and C (2pC), i.e. after the first pass, they were respectively rotated 90° or 180° around the extrusion axis direction (ED), Fig. 1e and f. The billet geometry and shear deformation underwent by a cubic element of material during the ECAP processing are schemat ically represented in Fig. 1d. Initially, the billet was introduced in the entrance channel in such a way that the plane normal to the transversal direction (TD) is the flow plane in exist channel, as shown in Fig. 1b. The billet, appropriately lubricated, was inserted in the die heated at the selected temperature using built in cartridge heaters. After each pass, the billets were water quenched.

Flat tensile samples with gauge dimensions 1.5 mm× 3 mm×20 mm were spark machined from the ECAP deformed billets with their longitudinal axis parallel to the extrusion direction as shown in Fig. 1c. Tensile tests at RT were carried out in an AG I Shimadzu machine at strain rates of $10^{-4}s^{-1}$ and $10^{-3}s^{-1}$. At least two ECAP treated samples, as well as two homogenized samples, were tested at each of the strain rates to ensure the reproducibility of the measurement and avoid misleading effects. The strain rate sensitivity of the samples was evaluated from the relationship:

$$m \quad \frac{\ln(\sigma_1/\sigma_2)}{\ln(\dot{\varepsilon}_1/\dot{\varepsilon}_2)} \qquad (1)$$

where $\sigma_1$ and $\sigma_2$ are the stress mean values at a strain of 0.06 in the true stress true strain curves for the strain rates $\varepsilon_1$ $10^{-4}s^{-1}$ and $\dot{\varepsilon}_2$ $10^{-3}s^{-1}$, respectively.

Metallographical analyses by optical microscopy (OM) and scanning electron microscopy (SEM) were performed on ECAP treated samples, as well as on homogenized samples, after being tensile deformed at RT. Graff Sargent and Keller re agents were used for revealing the microstructure.

In order to correlate the deformed microstructure with the SF characteristics of $\sigma$ $\varepsilon$ curves, specimens for transmission electron microscopy (TEM) were prepared from the samples tensile tested at RT. The specimens were electropolished at 15 V and 35 °C in a solution of 20% perchloric acid in ethanol. The TEM observations were carried out in a JEOL JEM 2032 microscope operated at 200 kV.

Texture measurements were performed on the longitudi nal plane of samples tensile tested up to fracture. The measurements were carried out in a Siemens diffractometer equipped with a D5000 goniometer. Incomplete (111) pole figures (PF) were recorded over a range of azimuthal angles $0°\leq\chi\leq80°$ in steps of $\Delta\chi$ $\Delta\Phi$ 5°. A textureless standard sample of pure Al was used for defocusing correction of the polar coordinates $\chi$ and $\Phi$.

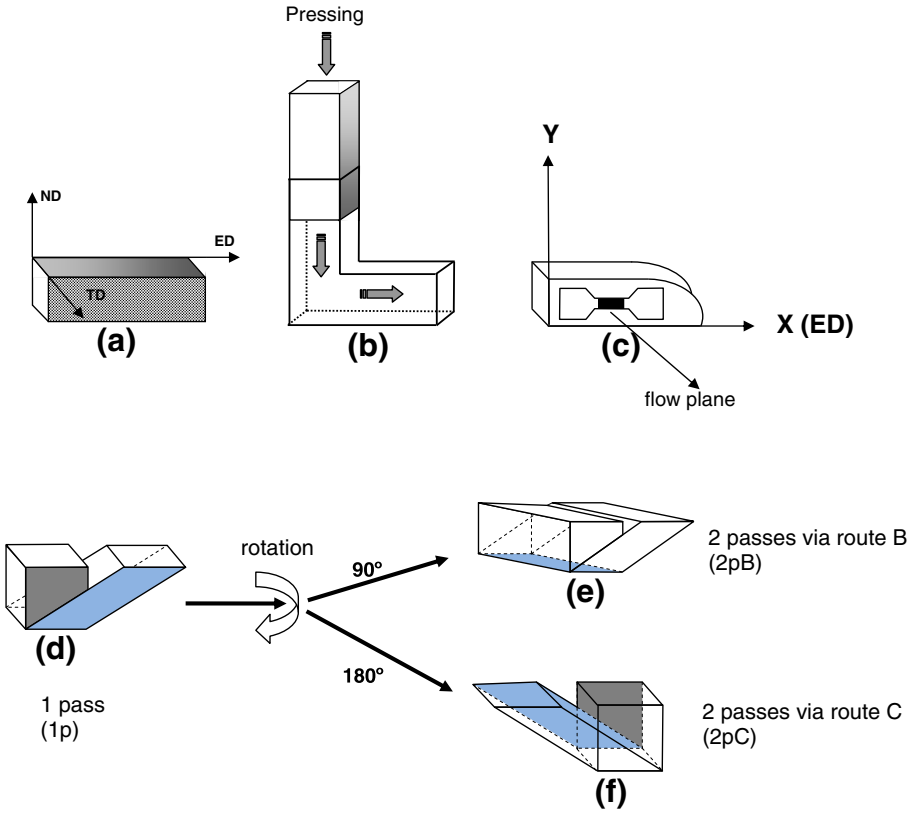


**Fig. 1 – Sketch showing the ECAP process: (a) starting ECAP billet, (b) 90° ECAP die, and (c) ECAP deformed billet and sample cut for tensile tests. Shearing of a cube element induced by (d) a single ECAP pass (1p) and two passes via (e) route B (2pB) or (f) route C (2pC).**

## 3. Results

### 3.1. *Initial Microstructure*

The microstructure and texture of the extruded PM Al 5Mg 1.2Cr alloy have been described in detail elsewhere [10]. For comparison, OM and TEM images of the grain structure and distribution of second phase particles in the homogenized alloy are shown in Fig. 2. The grain structure is coarse and elongated along the extrusion direction but fine grained zones, indicated by arrows, also appear as Fig. 2a and b reveals. These fine grained areas should have been developed by recrystallization during the extrusion process. It is impor tant noticing that the reagent causes preferential etching of the areas with higher stored energy. Then, the gray level in the OM images reveals the place where the plastic deforma tion and finer microstructure is located. These images show that the deformed zones are associated with a fine grained microstructure and a high density of the second phase particles. TEM images confirm that this initial microstructure is partially recrystallized as the large grains still contain deformation substructures composed by small subgrains associated with a fine dispersion of particles.

The texture of the homogenized microstructure is de scribed by a β fiber texture, i.e. an orientation tube running from the Cu orientation {112}⟨111⟩ through the S orientation {531}⟨112⟩ towards the Bs orientation {110}⟨112⟩ [10]. This texture is commonly observed in Al and Al alloys deformed at moderate and high temperatures.

### 3.2. *Flow Characteristics*

Fig. 3 shows the σ ε curves of the tensile tests for the homogenized and ECAP deformed samples performed at RT and strain rates of $10^{-4}s^{-1}$ and $10^{-3}s^{-1}$. All these curves after yielding reveal a remarkable SF up to fracture. The ECAP deformed samples tensile tested at $10^{-4}s^{-1}$, as well as the homogenized one, exhibit a single short serrated plateau preceded by the initial hardening after yielding, as it is indicated by arrows on the σ ε curves of Fig. 3a. This serrated plateau has been observed in the Al 5Mg alloy, and identified in the deformation range where a Lüders band forms and propagates [8], which corresponds to the Lüders strain. In contrast, the σ ε curves of the ECAP deformed samples tested at $10^{-3}s^{-1}$ reveal a characteristic succession of serrated plateaus, or stepwise stress jumps with regular stress oscillations superimposed as shown in Fig. 3b, d and f. This succession of plateaus does not appear in the σ ε curve of the homogenized alloy tested at $10^{-4}s^{-1}$. During the initial hardening stage after the plastic flow onset, stress oscillations of very small amplitude appear in all the σ ε curves. These stress oscillations, formerly reported in the Al 5Mg alloy [8,13], have been attributed to type A serrations produced by

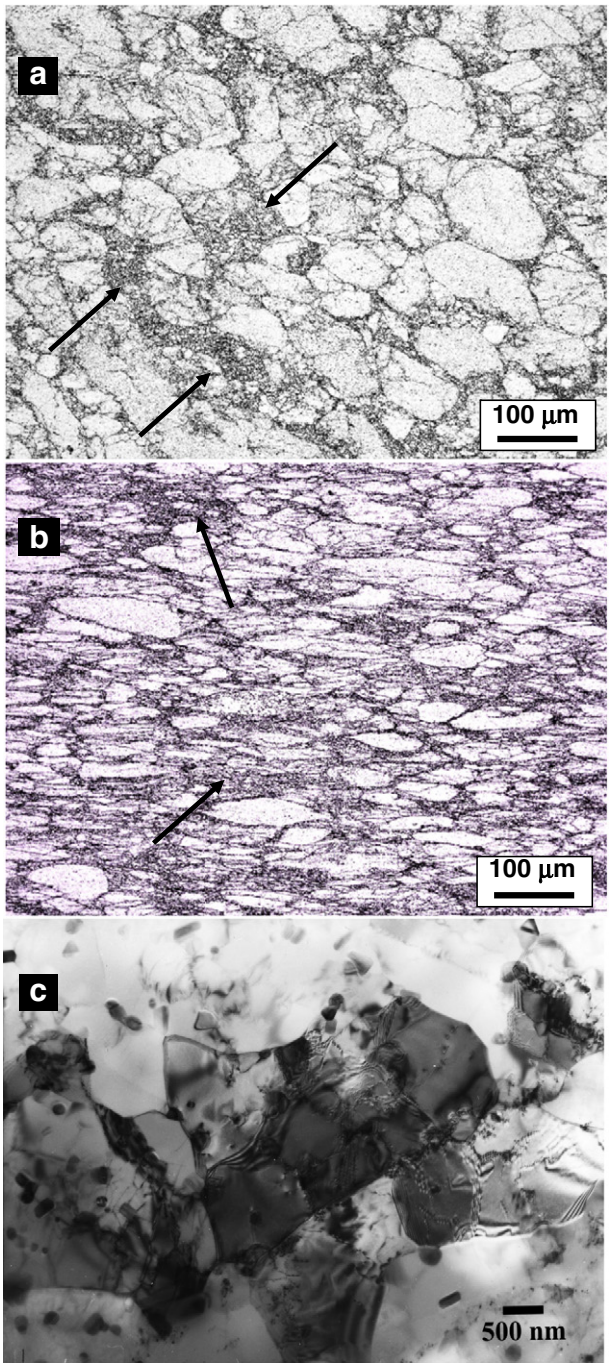


**Fig. 2 – Microstructure of PM Al–5Mg–1.2Cr in the homogenized condition: (a) OM image on a longitudinal plane, (b) OM image on a transversal plane and (c) TEM image showing the grain structure and the dispersion of the second phase particles.**

variations in the propagation rate of deformation bands that may be induced by imperfections in the sample surface. In the hardening stage following the initial one, the stress oscillations exhibit a behavior corresponding to type B serrations in agreement to the results reported for the Al 5Mg alloy tensile deformed in the strain rate range of $10^{-4}s^{-1}$ $10^{-3}s^{-1}$ [13]. Then, the $\varepsilon_c$ for the development of type B serrations appears to correspond to the Lüders strain of the first plateau detected in the $\sigma$ $\varepsilon$ curves just at the end of the initial hardening stage. Attention to these type B serrations is paid in the present work. The $\varepsilon_c$ values extracted from the $\sigma$ $\varepsilon$ curves are shown against ECAP temperature in Fig. 4. It is evident that $\varepsilon_c$ decreases with increasing ECAP temperature or tensile strain rate. Also, the same strain rate effect on $\varepsilon_c$ is observed for the homogenized alloy. It should be mentioned that this inverse dependence of $\varepsilon_c$ on strain rate has also been reported for some Al 5Mg alloys [32,33].

Fig. 5 shows the ECAP temperature and strain rate effect on the stress at the onset of type B like serrations $\sigma_c$. A drastic decrease of $\sigma_c$ with increasing ECAP temperature is evident, but the effect of the strain rate is rather ambiguous.

### 3.3. *Deformation Texture*

Fig. 6 shows the measured (111) PF for samples ECAP treated at 200 °C and 300 °C after being tensile tested at RT and strain rates of $10^{-4}s^{-1}$ and $10^{-3}s^{-1}$. It is expected that the tensile tests in the ECAP treated samples, irrespective of the strain rate, not produce any significant change in the crystallo graphic texture, since the strain to fracture in all the samples is quite smaller than the strain produced by the ECAP treatments, i.e. less of ~0.17 against ~1 produced by a single ECAP pass. However, some apparent changes are noted for samples processed at two ECAP passes.

A single ECAP pass at 200 °C (1p/200 °C) appears to induce the formation of the $(111)[\bar{2}5\bar{3}]$ orientation, as Fig. 6a and b reveal. In contrast, the texture induced in the samples treated at 2 ECAP passes via route B and 200 °C (2pB/200 °C treated samples) exhibits two components: $(114)[42\bar{3}] + (114)[\bar{4}5\bar{4}]$ for $10^{-4}s^{-1}$, and $(122)[2\bar{5}4] + (122)[\bar{2}\bar{1}2]$ for $10^{-3}$ $s^{-1}$, as shown in Fig. 6e and f, respectively. The texture of the 2pC/200 °C treated sample strained at $10^{-4}s^{-1}$ can be interpreted as $(254)[4\bar{4}3]$ orientation despite the apparent spreading of orientations toward the Y direction (Fig. 6i). In contrast, the texture of the 2pC/200 °C treated sample strained at $10^{-3}s^{-1}$ is similar to that developed in the 1p/200 °C sample, $(111)[\bar{2}5\bar{3}]$, (Fig. 6j).

The texture characteristics developed in the samples ECAP treated at 300 °C are somewhat different. The textures found in the 1p/300 °C samples, shown in Fig. 6c and d, are $(254)[4\bar{4}3]$ and $(111)[\bar{3}4\bar{1}]$ depending on if the strain rate was $10^{-4}s^{-1}$ or $10^{-3}s^{-1}$, respectively. In the 2pB/300 °C sample strained at $10^{-4}s^{-1}$ the texture found is $(111)[\bar{2}5\bar{3}]$ (Fig. 6g) but the $(132)[\bar{1}\bar{3}5]$ component appears in the sample strained at $10^{-3}s^{-1}$ as Fig. 6h reveals. The last orientation is related with the texture of 2pB/200 °C sample by a 35° rotation around a $\langle 111 \rangle$ axis. It should be mentioned that a weak $(235)[11\bar{1}]$ component is also observed in the 2pB/300 °C sample strained at $10^{-3}s^{-1}$. The measured PF in the samples 2pC/300 °C are shown in Fig. 6k and l. The $(423)[\bar{3}32]$ and $(112)[\bar{5}31]$ components are found in the sample strained at $10^{-4}s^{-1}$ while the texture in the sample strained at $10^{-3}s^{-1}$ is composed of the $(243)[30\bar{2}]$ and $(122)[\bar{2}01]$ components.

### 3.4. *Microstructure after RT Tensile Deformation*

ECAP deformation induces the refinement of the initial microstructure by grain fragmentation and the second phase

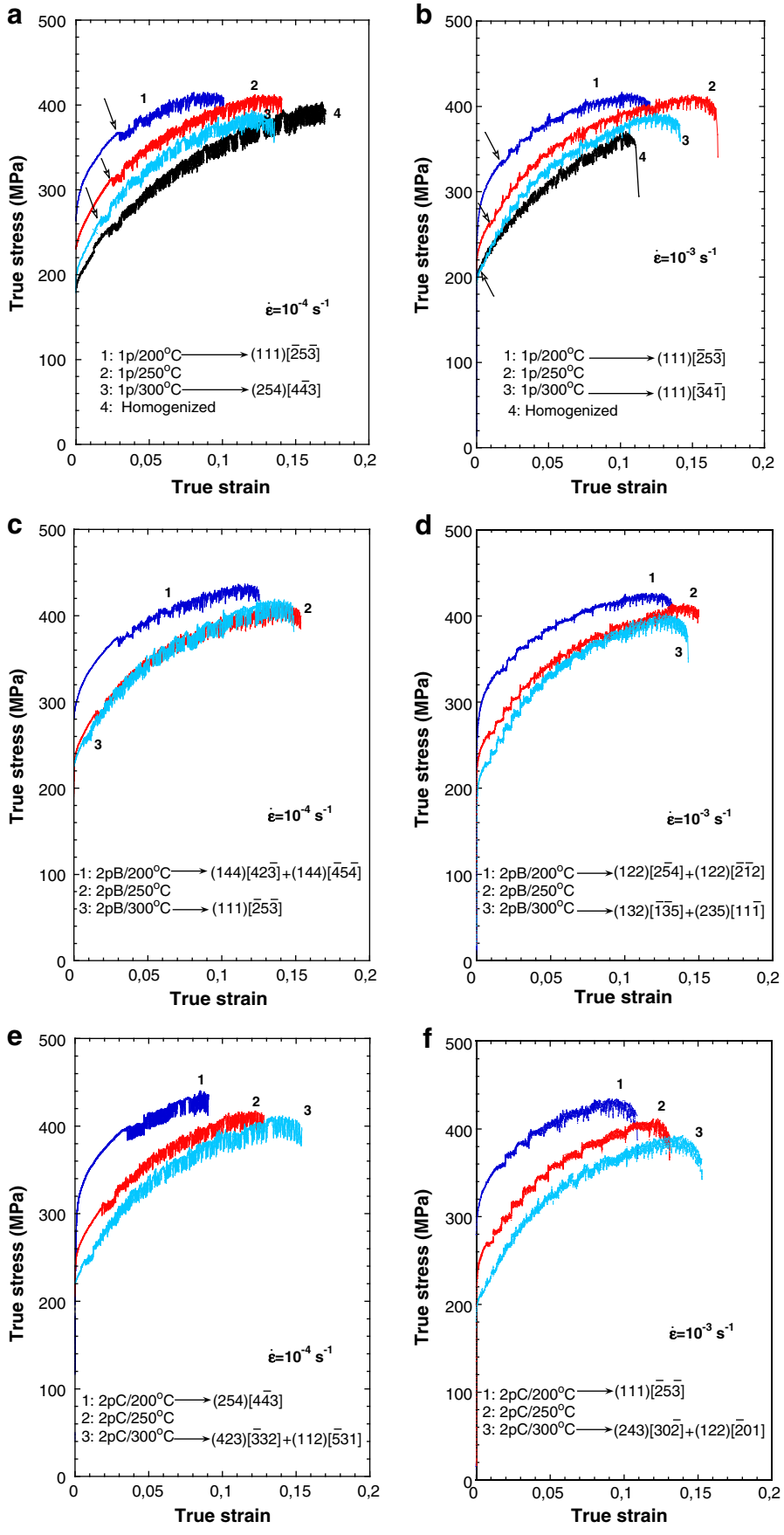
a
True stress (MPa)
True strain
1
2
3
4
ε̇=10^-4 s^-1
1: 1p/200°C → (111)[2̄53̄]
2: 1p/250°C
3: 1p/300°C → (254)[44̄3]
4: Homogenized
b
ε̇=10^-3 s^-1
1: 1p/200°C → (111)[2̄53̄]
2: 1p/250°C
3: 1p/300°C → (111)[34̄1̄]
4: Homogenized
c
ε̇=10^-4 s^-1
1: 2pB/200°C → (144)[42̄3̄]+(144)[4̄54̄]
2: 2pB/250°C
3: 2pB/300°C → (111)[2̄53̄]
d
ε̇=10^-3 s^-1
1: 2pB/200°C → (122)[2̄54̄]+(122)[2̄1̄2̄]
2: 2pB/250°C
3: 2pB/300°C → (132)[1̄3̄5̄]+(235)[11̄1̄]
e
ε̇=10^-4 s^-1
1: 2pC/200°C → (254)[44̄3]
2: 2pC/250°C
3: 2pC/300°C → (423)[3̄32]+(112)[5̄31]
f
ε̇=10^-3 s^-1
1: 2pC/200°C → (111)[2̄53̄]
2: 2pC/250°C
3: 2pC/300°C → (243)[302̄]+(122)[2̄01]

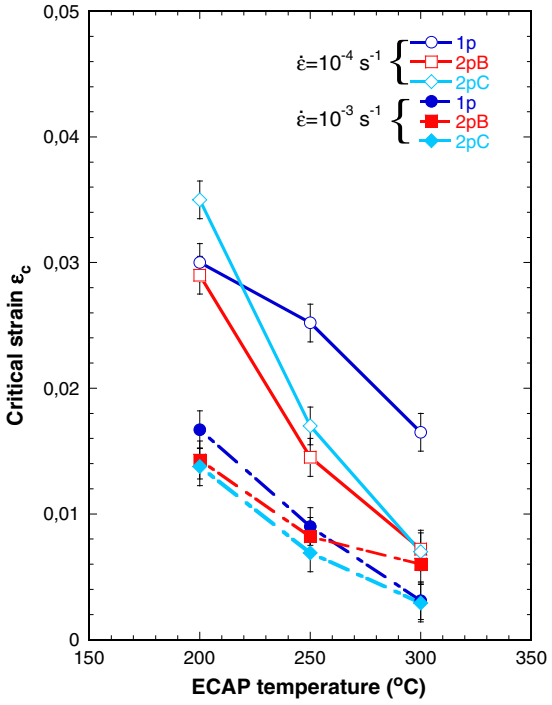


**Fig. 4 – Effect of the ECAP temperature and strain rate on the critical strain for the onset of type B serrated flow in the Al–5Mg–1.2Cr alloy.**

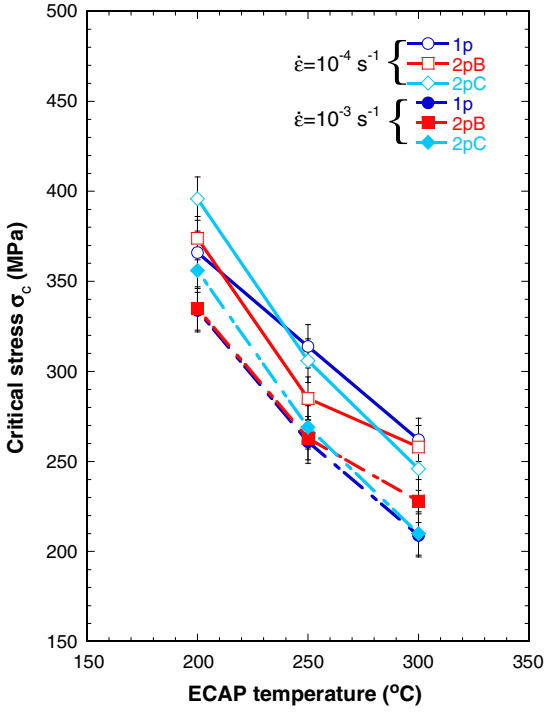


**Fig. 5 – Effect of the ECAP processing on the critical stress for onset of type B serrations in the Al–5Mg–1.2Cr alloy.**

particles redistribution. The ECAP treatment at 200 °C pro duced a microstructure finer than the ones observed in the homogenized material or after ECAP deformation at 300 °C. The slight coarsening of the microstructure observed at 300 °C is due to the recovery enhancement at this temperature, which decreases the stored energy preventing therefore grain refinement. In order to assess the effect ECAP deformation on the flow characteristics of the Al 5Mg 1.2Cr alloy after RT tensile deformation, the microstructure was examined in the gauge and grip regions of the tensile strained samples. The microstructures observed in strained regions were only slightly finer than those in unstrained areas were.

A general view of the microstructures for the samples ECAP deformed at 200 °C after being tensile strained at RT, along with those corresponding to the homogenized material, are shown in Fig. 7. The microstructure of the homogenized material strained up to fracture at $10^{-4}$ s$^{-1}$ and $10^{-3}$ s$^{-1}$ is shown for comparison in Fig. 7a and b, respectively. The grain structure is clearly elongated along the tensile axis. The first ECAP pass produces a fairly equiaxial grain structure homogeneously deformed, see Fig. 7c and d. OM close images showing traces of SBs and the interaction of deformation with grain boundaries and particles are shown in Fig. 9a. The grain structure in the 2pB/200 °C is elongated along a direction ~15° inclined respect to the tensile axis. A general characteristic of these microstructures is the effect of SB propagation on recrystallized areas surrounding the grain boundaries, especially, those boundaries parallel to the short axis of the grains as indicated by arrows in Figs. 7e a n d 9b. The 2pC/200 °C sample tensile strained at $10^{-4}$ s$^{-1}$ exhibits a microstructure slightly coarser than the corresponding one developed in the 1p/200 °C sample, compare Fig. 7g a n d c . I n contrast, when a 2pC/200 °C sample is deformed at $10^{-3}$ s$^{-1}$ the opposite occurs, besides exhibiting a severely deformed micro structure and perceptible SB traces alike to those observed in the 1p/200 °C sample strained at $10^{-4}$ s$^{-1}$ (Fig. 7h).

Fig. 8 shows the microstructure of the material ECAP processed at 300 °C. Now, the microstructure appears to be less differentiated each other, and apparently coarser than the corresponding to the samples ECAP treated at 200 °C, compare Fig. 8a and e to Fig. 7c and g, respectively. A similar effect of SB propagation on the microstructure is observed as shown in Fig. 9c and d.

Fig. 10 shows SEM images that reveal the interaction of SBs with the second phase particles in the homogenized material tensile tested at RT at $10^{-4}$ s$^{-1}$. These second phase particles have been identified elsewhere as $Al_{18}Mg_3Cr_2$ [34]. I t w a s observed that the initial bands nucleated at the curved ends of the sample gauge region, where a high stress concentration should be developed, and propagated toward the opposite end. These bands during their propagation can be either temporally retained or completely arrested by obstacles. In this last case, a

**Fig. 3 – σ–ε curves for the ECAP deformed Al–5Mg–1.2Cr alloy tensile tested at RT and strain rates of $10^{-4}$s$^{-1}$ and $10^{-3}$s$^{-1}$: (a, b) a single ECAP pass (1p), (c, d) two ECAP passes via route B (2pB); (e, f) two ECAP passes via route C (2pC). The σ–ε curves for the homogenized alloy are included for comparison. The arrows indicate the onset of the type B serrations. The texture is also included for comparison.**

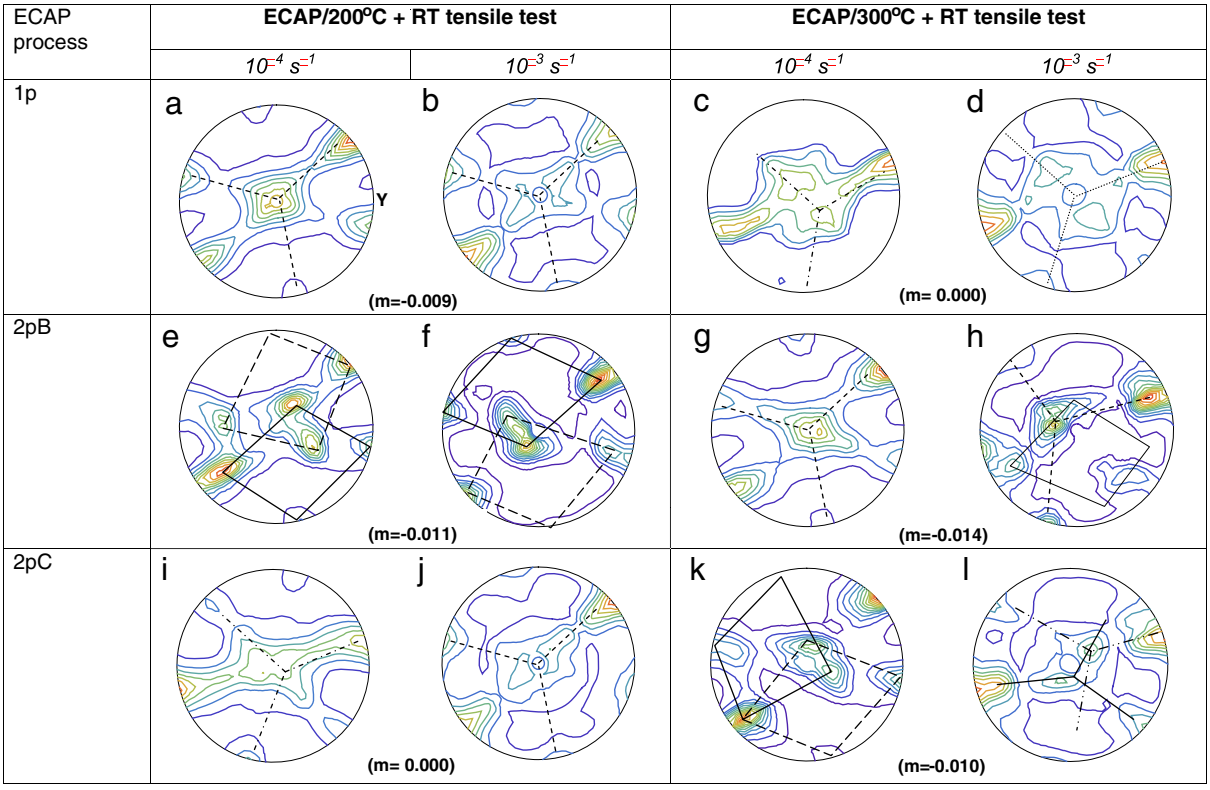


**Fig. 6 – (111) PF showing the crystallographic texture, and the strain rate sensitivity value *m*, for ECAP deformed Al–5Mg–1.2Cr after being tensile strained up to fracture at $10^{-4}s^{-1}$ and $10^{-3}s^{-1}$. The *m* value is determined from Eq. (1).**

new front of a new band, initiated at any of the ends of the sample gauge region, would move toward the opposite one. Then, a halting band propagation yields the serrations observed in σ ε curves. A remarkable feature of the band structure is the zigzag band fronts developed on the sample surfaces due to the interaction of the bands with the second phase particles as Fig. 10b reveals. Also, the interaction between SBs gives rise to a characteristic cross banded structure with intersection angles of ~70° as the images in Fig. 10a and c show.

The SB structures induced by tensile deformation at RT in the samples ECAP processed at 200 °C and 300 °C are shown in Fig. 11. They are comparable to the ones developed in the homogenized alloy irrespective of the ECAP conditions and tensile strain rate. The bands are found oriented about 45° in respect to the tensile axis, and spread all over the grains in the whole gauge region as observed for the case of the homoge nized material.

### 3.5. *TEM Observations*

The microstructure of the tensile tested samples revealed by TEM was alike for all the samples irrespective of the treatment underwent before testing. Fig. 12 shows the microstructure of the alloy tensile deformed at $10^{-4}$ $s^{-1}$, in the homogenized condition and after being ECAP treated. In all the cases, plastic deformation was found confined in extensive areas containing a very high density of dislocations. Deformation zones associated with the second phase particles present in the alloy are frequently observed as the images of Fig. 12 reveal. These TEM images evidence the interaction between the SBs and the particles, i.e. band pinning and release by particles as the SEM image in Fig. 11b shows. It should be mentioned that neither development of a subgrain structure nor particle shearing and void formation at the particle/matrix interface are found in the tensile deformed samples.

## 4. Discussion

### 4.1. *Strain Rate Effect*

The microstructure of the extruded PM Al 5Mg 1.2Cr alloy in the homogenized condition is composed by coarse elongated grains containing substructure and small recrystallized grains (Fig. 2). Neither dissolution nor precipitation of the second phase particles is expected to occur during the ECAP treatments or tensile tests as has been confirmed by differential scanning calorimetry [34]. The σ ε curve for the alloy in the homogenized condition shows serrations starting at around the onset of the plastic deformation (Fig. 3). Then, no critical plastic strain appears to be needed to trigger the SF in this case. Apparently, these serrations are similar to the type B serrations frequently reported in Al Mg alloys undergoing the PLC effect. It was attributed to parallel bands going across the entire gauge region of the sample resulting in a surface relief without formation of micro shear bands [13]. However, the surface of the homogenized material

after tensile deformation at RT exhibits quite different structural features, i.e. groups of SBs passing across the grains along different directions, and microbands in some isolated zones. Moreover, the SB fronts show a zigzag path due to their interaction with the second phase particles, as shown in Fig. 11b and c. This indicates that the flow instabilities in the alloy under the present testing conditions may be affected by the interaction of SBs with the second phase particles. Then, the SF behavior in this alloy cannot be exclusively explained in terms of the solute dislocation interaction suggesting that shear banding and particles play a fundamental role in the SF behavior of the $\sigma$ $\varepsilon$ curve.

The interaction of SBs with particles in the Al 5Mg 1.2Cr alloy points out that both the particle size and the inter particle

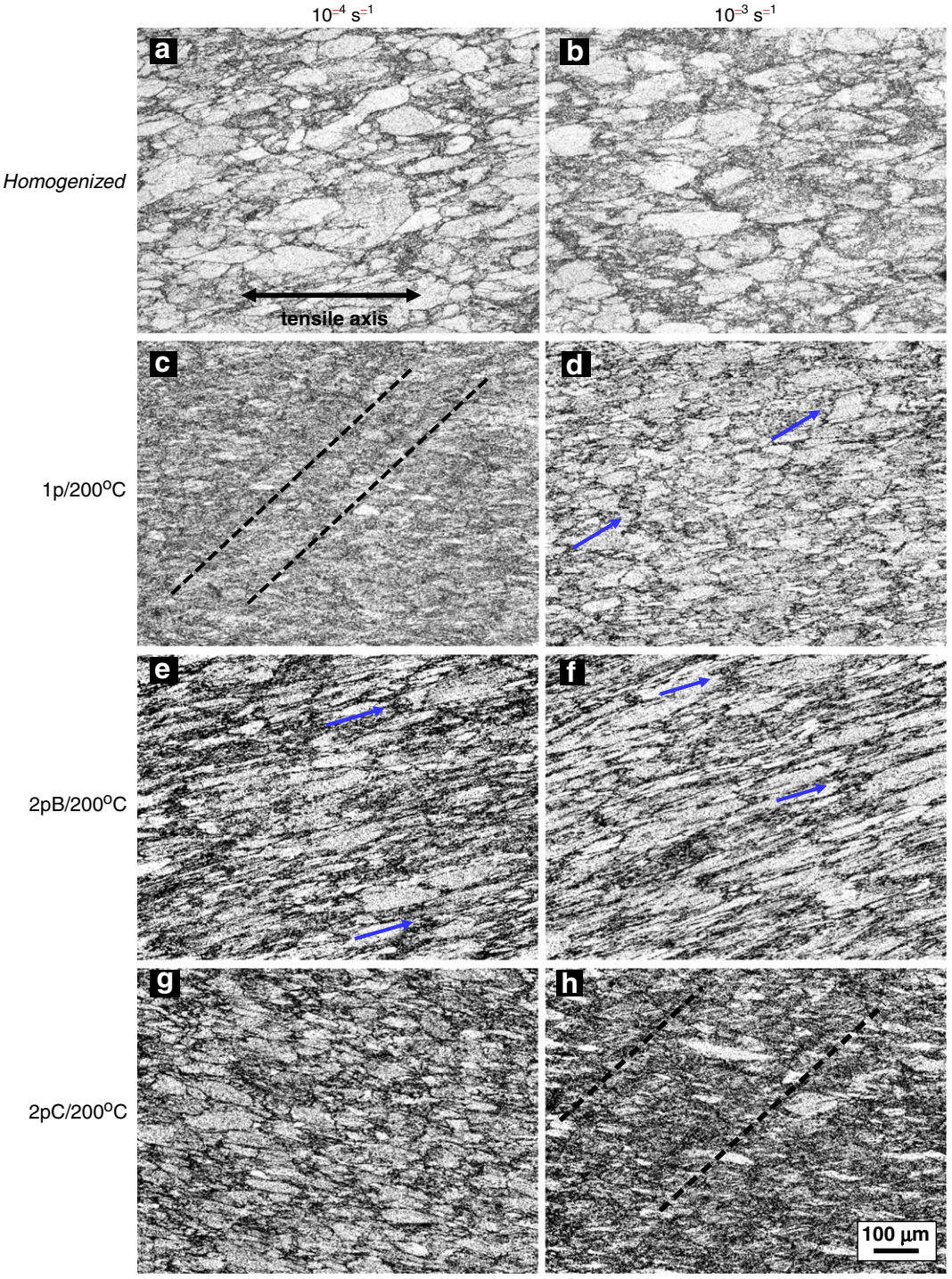


**Fig. 7 – OM images of the etched microstructures of Al–5Mg–1.2Cr ECAP treated at 200 °C and in the homogenized condition, tensile strained up to fracture at $10^{-4}s^{-1}$ and $10^{-3}s^{-1}$. The discontinuous lines indicate SBs traces.**

spacing may control the SF. If it is tentatively assumed that plastic flow is produced by thermally activated propagation of the band, the strain rate would be given by the equation [14]:

$$\dot{\varepsilon} \quad \frac{\Omega}{t_w} \tag{2}$$

where $\Omega$ is the plastic strain produced by a band moving to the next obstacle, and $t_w$ the waiting time of the band for surmounting the obstacles that would be given by

$$t_w \quad v_0^{-1} \exp(\Delta E/kT) \tag{3}$$

where $v_o$ is the attempt frequency, $\Delta E$ the average energy barrier to be surmounted by the moving band at the obstacles, $k$ the Boltzmann constant and $T$ the sample temperature. Then, the strain rate can be expressed by:

$$\dot{\varepsilon} \quad v_o \Omega \exp(\ \Delta E/kT). \tag{4}$$

The obstacle strength for the bands and the local stress acting at the band front would determine the value of $\Delta E$, and the waiting time $t_w$ for a given temperature would decrease with increasing strain rate according to the above equations. Thus, for a given temperature, $\Delta E$ value at a strain rate of $10^{-3}s^{-1}$ should be smaller than the one for a strain rate of $10^{-4}s^{-1}$, i.e. the strength of the obstacles decreases with in creasing strain rate and lowering the amplitude of the stress oscillations in the flow stress curve. This explains the present results for the homogenized and ECAP processed material in relation with the strain rate effect on the serration amplitude.

Now, the severe plastic deformation effect on the features of the SF will be considered. The main features resulting from the analysis of the $\sigma$ $\varepsilon$ curves are summarized as follows:

i. Two distinguishable features in the $\sigma$ $\varepsilon$ curves have been found depending on the strain rate: the initial hardening

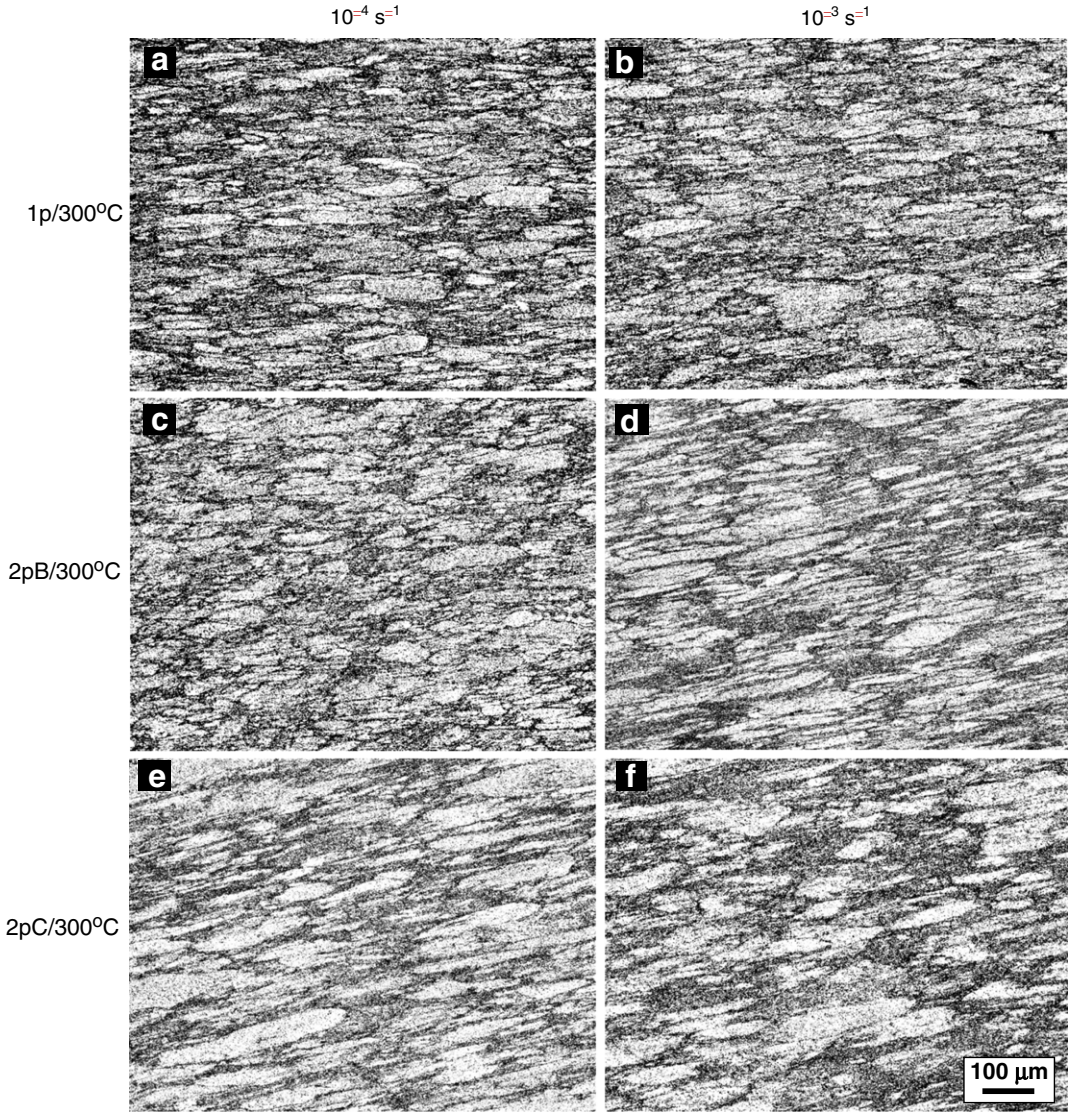


**Fig. 8 – OM close view images of the etched microstructures induced in ECAP treated Al–5Mg–1.2Cr after being tensile strained up to fracture at $10^{-4}s^{-1}$ and $10^{-3}s^{-1}$.**

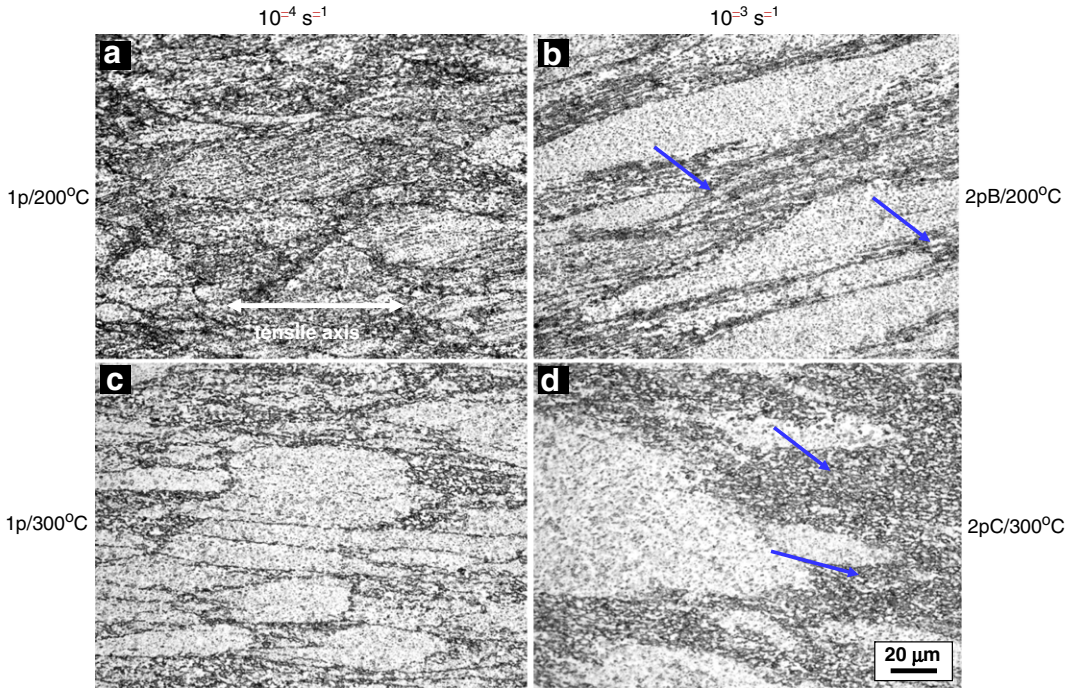


**Fig. 9 – OM images of the etched microstructures in Al–5Mg–1.2Cr ECAP treated at 300 °C and tensile strained up to fracture at $10^{-4}s^{-1}$ and $10^{-3}s^{-1}$.**

region is followed by either SF with continuous strain hardening until failure at a strain rate of $10^{-4}s^{-1}$ or a succession of plateaus with SF superimposed at $10^{-3}s^{-1}$.

ii. A critical strain $\varepsilon_c$ (or stress $\sigma_c$) for the onset of type B serrations is observed at strain rates of $10^{-4}s^{-1}$ and $10^{-3}s^{-1}$, which decreases with increasing ECAP temperature or strain rate.

iii. The serration amplitude increases with increasing strain, and attains a saturation value near the fracture strain.

SF occurs under the effect of the applied and the internal stresses [7,35]. Therefore, the internal stresses produced by the severe plastic deformation may have an effect on the mode of nucleation and propagation of the bands. The stress value for $\varepsilon_c$ is the threshold stress $\sigma_c$ beyond which SBs form during tensile deformation, and move along the shear plane through the gauge region of the sample. For a given ECAP route and number of passes, the decrease of $\sigma_c$ with increasing ECAP temperature (5) is attributable to the dynamic recovery and rearrangement of dislocations during the ECAP deformation, which would be stronger at higher processing temperature. As a result, in the samples ECAP treated at 200 °C, the contribution of the internal stresses to the local effective stress for band nucleation and propaga tion should in general be smaller all over the samples requiring a higher applied stress. However, the internal stresses in the samples ECAP deformed at higher temper atures would be localized at the dislocation walls so that the threshold stress for band nucleation would attained under smaller applied stresses at the regions with disloca tion rearrangement.

On the other hand, the strain rate sensitivity $m$, evaluated from the $\sigma$ $\varepsilon$ curves at $10^{-4}s^{-1}$ and $10^{-3}s^{-1}$ using Eq. (1), i sc bs e to zero or negative depending on the ECAP processing condi tion. These $m$ values are shown, along with the texture results in Fig. 6 in order to find some plausible correlation between texture and strain rate sensitivity. The 1p/200 °C, 2pC/200 °C and 1p/300 °C samples exhibit values of $m$ 0, and the rest $m<0$. These results suggest that the texture induced by ECAP, as well as the microstructure, could have capability to lower the $m$ value to negative values. It should be mentioned that a decrease of the strain rate sensitivity with increasing strain induced by cold work has been reported for the 5086 AA alloy [36].

### 4.2. *Texture Effects*

Now, let us check the relationship between the ECAP conditions and the mechanical characteristics of SF in $\sigma$ $\varepsilon$ curves. For the material ECAP treated at 200 °C, the 2pC/200 °C sample tensile strained at $10^{-4}s^{-1}$ exhibits a high SF ampli tude, and $\varepsilon_c$ and $\sigma_c$ values higher than the corresponding values for the 1p/200 °C and 2pB/200 °C samples (see Figs. 4 and 5). In contrast, the elongation to failure $\varepsilon_f$ is low. This discrepancy is, in principle, associated with the deformed microstructure and texture. The grain structure of the 2pC/ 200 °C sample is quite fine and its preferential orientation $(254)[4\bar{4}3]$, which has only two active slip systems. On the contrary, the samples 1p/200 °C with orientation $(111)[\bar{2}5\bar{3}]$ and the 2pB/200 °C samples with orientations $(114)[42\bar{3}]$ and $(114)[45\bar{4}]$ would have four and five slip systems, respective ly. Also, the samples ECAP treated at 300 °C and strained at $10^{-4}s^{-1}$ exhibit a similar variety of preferential orientations and active slip systems, along with similar SF characteristics.

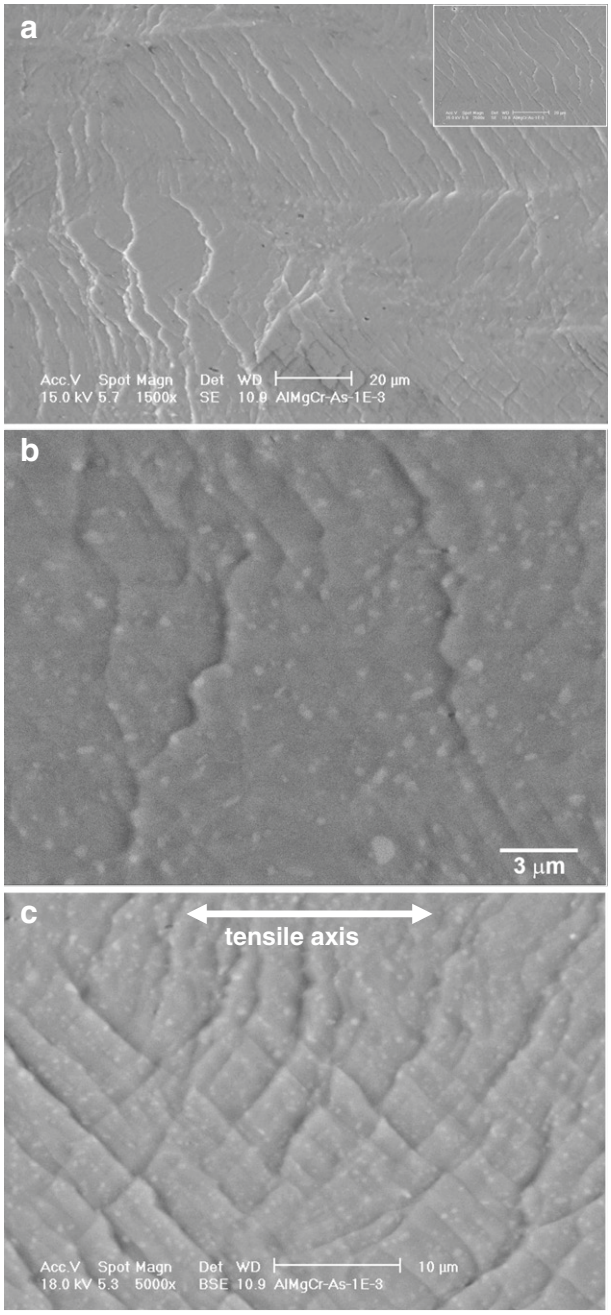


**Fig. 10 – SEM images showing the structure of SBs in the homogenized Al–5Mg–1.2Cr alloy tensile tested at RT and strain rate of $10^{-4}s^{-1}$: (a) band fronts propagated along different directions; the inset shows details of parallel bands, (b) interaction of SBs with the second phase particles and (c) cross-banded structure inside a grain.**

For instance, the 1p/300 °C sample with preferential orientation $(254)[4\bar{4}3]$ exhibit high $\varepsilon_c$ and $\sigma_c$ values and low $\varepsilon_f$ like the 2pC/200 °C sample. Moreover, the 1p/300 °C samples having two active slip systems developed a grain structure elongated along the tensile axis, but the samples 2pB/300 °C and 2pC/300 °C with four or five slip systems show grain elongation along an axis clearly rotated respect to the tensile axis (Fig. 8c and e). All the above suggests a correlation between the crystallographic texture and the characteristics of the SF of the samples ECAP treated at a given temperature, i.e. the lower the number of slip systems the higher the critical strain for the SF and the lower the strain to failure. However, the result comparison between the samples ECAP treated at the same temperature does not confirm such correlation irrespective of the strain rate. When the results for samples ECAP treated at the different temperatures are compared, those exhibiting identical textures, or nearly the same, do not yield comparable $\varepsilon_c$, $\sigma_c$ and $\varepsilon_f$ values, nor SF characteristics, as the corresponding $\sigma$ $\varepsilon$ curves shown in Fig. 3 reveal.

The above indicates that the effect of texture on the SF of the ECAP treated Al 5Mg 1.2Cr alloy results to be ambiguous, and therefore, the grain structure in conjunction with the characteristics of the second particles particle would be the factors controlling the SF of the alloy tensile strained under the present conditions.

### 4.3. *Effects of the Grain Structure and Second-Phase Particles*

The $\sigma$ $\varepsilon$ curves of the ECAP processed samples tested at a strain rate of $10^{-3}$ $s^{-1}$ exhibit a succession of serrated plateaus (Fig. 3b, d and f). Similar plateaus have also been observed in other Al alloys although their origin has not been clearly established. For instance, the $\sigma$ $\varepsilon$ curves of the pre deformed Al 5Mg 0.8Mn alloy exhibited SF on a sequence of plateaus. These plateaus did not appear for non pre deformed samples that showed SF accompanied by continuous strain hardening [37]. The development of plateaus in $\sigma$ $\varepsilon$ curves for Al Mg alloys has also been associated with generation of bands, and each oscillation superimposed on the plateaus would corre spond to formation of a moving band ahead of a prior one that has been pinned by obstacles [38].

Fig. 13 illustrates schematically a mechanism proposed to account for the SF characteristics of the ECAP treated Al 5Mg 1.2Cr alloy in conjunction with the evolution of the microstructure. It is assumed that the most plausible sites for the nucleation of the first band are the ends of the sample gauge region due to high concentration of stresses that would be developed at these curved ends [39]. In fact, the appearance of the first moving SB during the tensile tests was observed at one of the ends of the sample gauge region. The hard particles in the matrix represent obstacles for the band propagation. The formation of the first plateau observed in all $\sigma$ $\varepsilon$ curves is attributed to the nucleation of this first SB and its propagation toward the opposite one (Fig. 13a). This band during its propagation would interact with particles and shear the grains favorably oriented respect to the tensile axis, i.e. those grains with a high Schmid factor for which the resolved shear stress would be high enough for band propagation [7]. The band moves on the glide planes of a grain until it runs into a grain boundary. If the adjacent grains are favorably oriented to activate dislocation slip on a glide plane, then the band propagation would continue. On the contrary, if this condition is not satisfied, the band remains hindered by the obstacles until the effective stress, or applied strain, gives rise to a favorable dislocation arrangement to surpass the obstacle. A new band would not form during the expansion of the plateau although stress oscillations superimposed on the plateau appear due to the action of the effective stress on a prior band hampered by the grain boundaries and second phase particles.

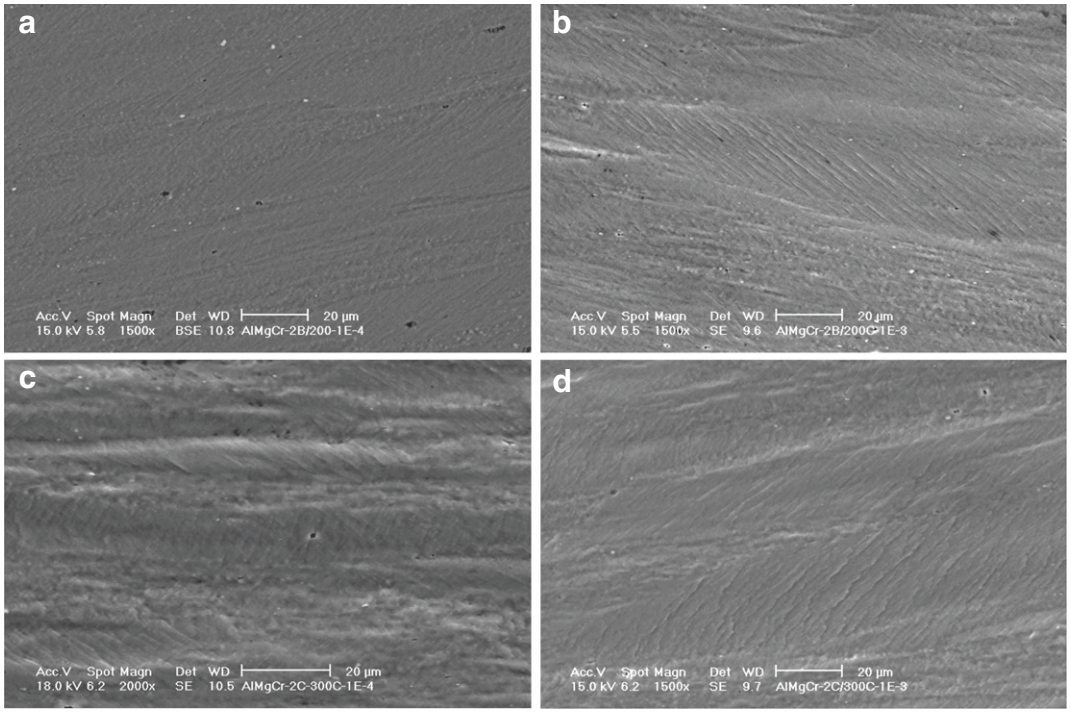


**Fig. 11 – SEM images showing the structure of SBs in the ECAP processed Al–5Mg–1.2Cr alloy tensile tested at RT: (a, b) 2pB/200 °C samples tensile tested at strain rates of $10^{-4}s^{-1}$ and $10^{-3}s^{-1}$, respectively. (c, d) 2pC/300 °C samples tensile tested at $10^{-4}s^{-1}$ and $10^{-3}s^{-1}$, respectively.**

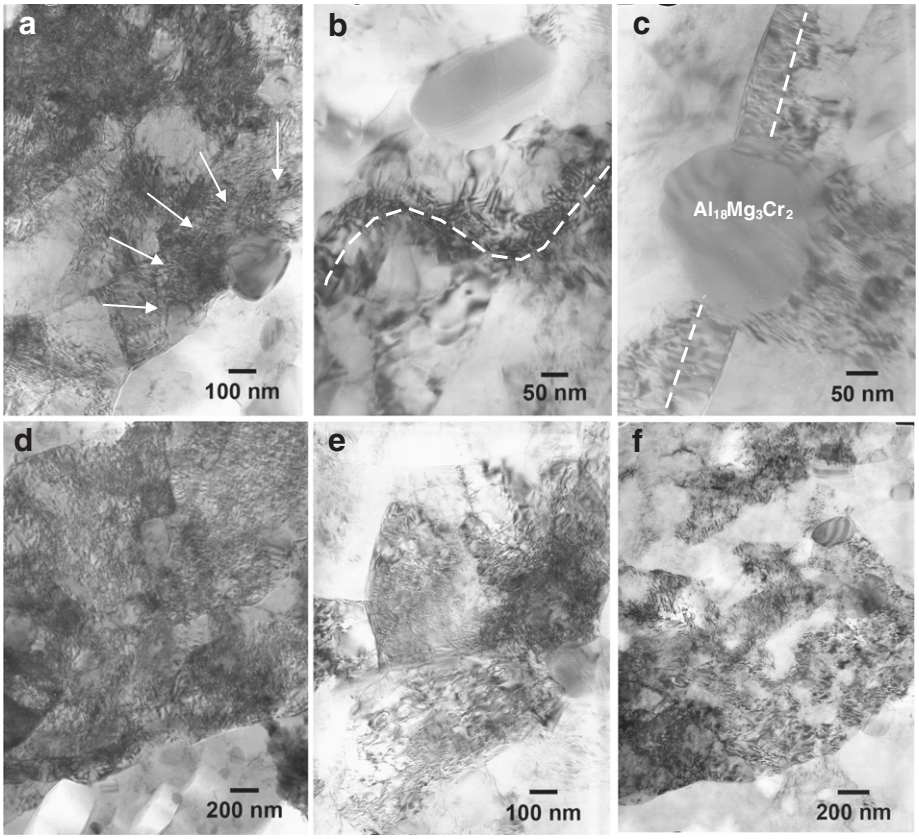


**Fig. 12 – TEM images showing areas of plastic deformation zones associated with the second phase particles in the Al–5Mg–1.2Cr alloy tensile tested at RT at $10^{-4}s^{-1}$: (a)–(c) samples in the homogenized condition and (d)–(f) 2pC/250 °C samples.**

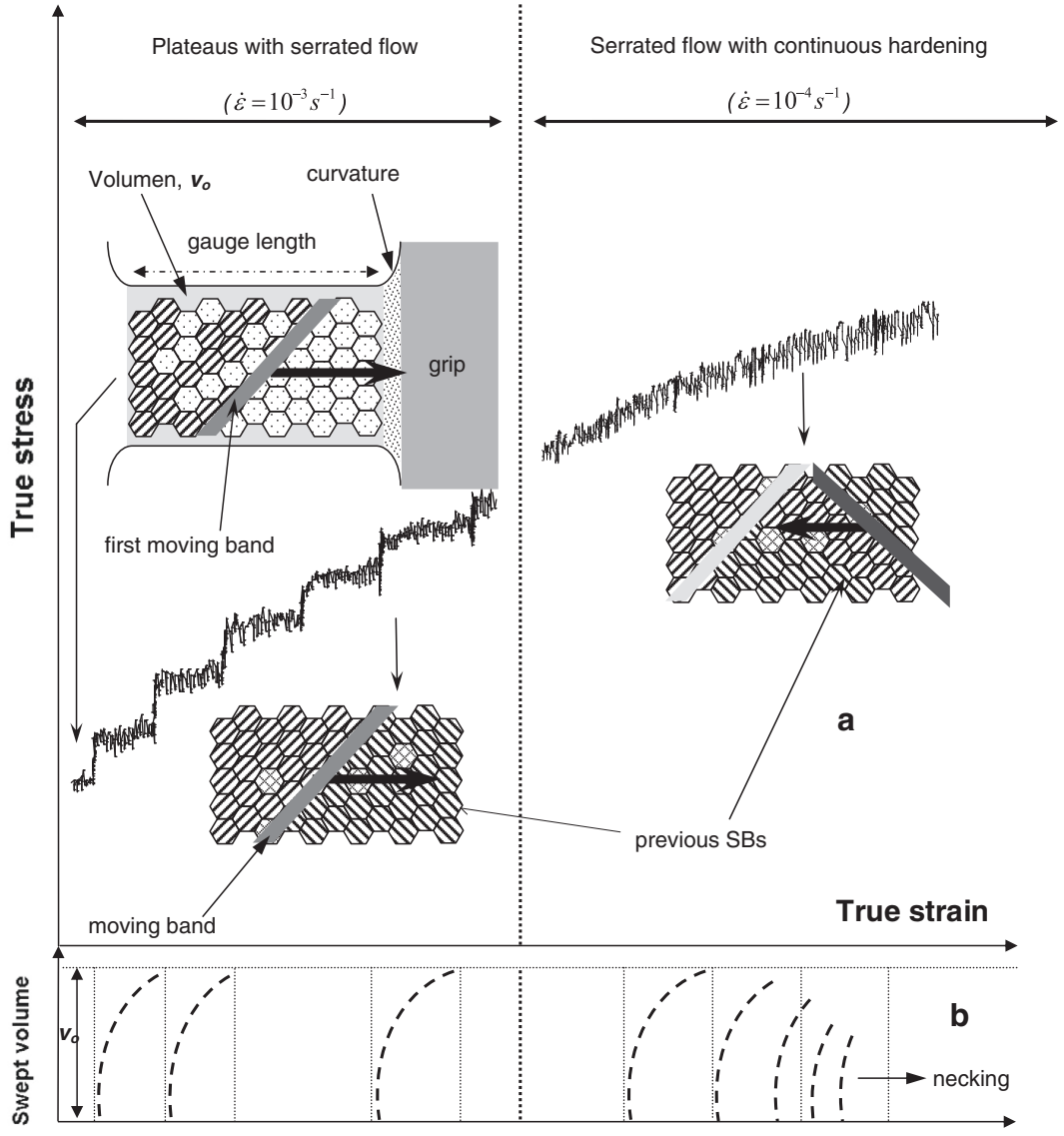


**Fig. 13 – Outline describing the propagation mechanism of the SBs in the Al–5Mg–1.2Cr alloy tensile tested at RT that accounts for the variation of the SF features induced by a change in the strain rate: (a) interaction of the moving SBs with the grains along the sample gauge length and (b) representation of the volume swept ($V_o$) by the moving SBs during the deformation cycle of a band.**

When the plateau in the σ ε curve is over, the moving band there will sweep a determined volume of sample, $V_o$ in Fig. 13b, which means that a deformation banding cycle of grains has just been accomplished. The stress jump from a plateau to the next one indicates that a threshold stress is required to activate a new band at one of the ends of the sample gauge region. Then, the new plateau appears in the σ ε curve giving rise to other deformation banding cycle. This would induce cross banding in grains initially sheared and plastic deformation in unsheared grains. Later on, as the applied strain increases, the nucleation probability of SBs also increases all over the gauge region of the sample; i.e. the threshold stress for band nucleation lowers and the new SBs form faster. Now, beyond certain tensile strain a new band forms and moves before the prior one completes its propagation. This reduces the volume swept by each moving band during its deformation cycle and makes less appreciable the plateaus in the σ ε curves as schematically outlined in Fig. 13b. As the applied strain still increases more, the sample volume swept by the successive SBs becomes gradually smaller. This produces the disappearance of visible plateaus, and thus the saturation of the stress oscillations and failure of the sample. All of the above account for the SF behavior of the samples tested at $10^{-3}s^{-1}$.

For the samples tested at $10^{-4}$ $s^{-1}$, the σ ε curves (Fig. 3a, c and e) exhibit SF with continuous hardening just after the completion of the Lüders stage. No plateaus are observed in this regime, apparently. The SF behavior in this case is similar to that observed for the samples tested at $10^{-3}s^{-1}$ after completion of the plateaus stage. Thus, the corresponding mechanism proposed for the samples tested at $10^{-3}s^{-1}$ can be extrapolated to explain the SF with continuous hardening at $10^{-4}s^{-1}$. At this strain rate, the velocity of mobile dislocations is expected to be low enough to allow a more homogeneous distribution of deformation in comparison to the strain rate of $10^{-3}s^{-1}$. Then, the plastic flow should be practically distributed in the entire volume of the deformed sample, and much more potential sites for the band nucleation there would be all along the gauge region

of the sample. Although the nucleation of the first band is expected at the ends of the sample gauge region, the following bands may be nucleated all over the gauge region. However, the nucleation of a new band in this case occurs before the preceding band finishes its deformation cycle. Increasing applied strain, the successive bands would sweep less volume and the cycle of deformation banding would become shorter. At this stage, plastic flow instability may be attained in some areas of the gauge region resulting in necking and failure of the sample.

## 5. Conclusions

The microstructure and mechanical behaviors at room temperature of extruded PM Al 5Mg 1.2Cr processed by ECAP have been investigated. The main conclusions are summarized as follows:

1. The alloy ECAP processed in the temperature range of 200 300 °C, as well as in the homogenized condition, exhibited SF when it was tensile deformed at room temperature. The threshold stress and strain for the serration onset decreased with increasing ECAP temperature or strain rate.
2. All the samples ECAP processed and tensile tested under the present conditions developed shear banding. Interaction of the SBs with the second phase particles was observed. The $\sigma$ $\varepsilon$ curves for the ECAP processed samples show a transition from SF with continuous strain hardening to SF superimposed to a sequence of constant stress plateaus, when the strain rate is changed from $10^{-4}s^{-1}$ to $10^{-3}s^{-1}$.
3. The plateaus in $\sigma$ $\varepsilon$ curves developed at a strain rate of $10^{-3}s^{-1}$ were ascribed to the nucleation of a band at one end of the sample gauge region and its subsequent propagation towards the opposite one, i.e. to a cycle of deformation banding. The following plateau was associated with the nucleation of a new band in one end of the sample gauge region and its propagation.
4. At a low strain rate of $10^{-4}s^{-1}$ the sites for band nucleation should be randomly distributed along the gauge region of the sample. The disappearance of the plateaus and continuous strain hardening in the $\sigma$ $\varepsilon$ curves are attributed to the activation of a new moving band before the completion of the deformation banding cycle of the preceding band.
5. No obvious relationship between the texture and the SF characteristics has been found.

## Acknowledgments

The experimental work has been carried out at the LMNM (LM 290) laboratory supported by Madrid Community through the project TECHNOFUSION (S2009/ENE 1679) and Spanish Ministry of Science and Innovation (contract ENE2008 06403 C06 04).

## REFERENCES

[1] Hayes RW, Hayes WC. A proposed model for the disappearance of serrated flow in two Fe alloys. Acta Metall 1984;31:259 67.
[2] Pink E, Kumar S. Patterns of serrated flow in low carbon steel. Mater Sci Eng A 1995;201:58 64.
[3] Hayes RW. On a proposed theory for the disappearance of serrated flow in fcc Ni alloys. Acta Metall 1983;31:365 71.
[4] Dziadon A. The effect of grain size on serrated flow of nickel. Scr Mater 1996;34:375 80.
[5] Mohamed FA, Murty KL, Langdon TG. The Portevin Le Châtelier effect in CuAu. Acta Metall 1974;22:325 32.
[6] Hayes RW. The disappearance of serrated flow in two copper alloys. Mater Sci Eng 1986;82:85 92.
[7] Fujita H, Tabata T. Discontinuous deformation in Al Mg alloys under various conditions. Acta Metall 1977;25:793 800.
[8] Robinson JM, Shaw MP. Observations on deformation characteristics and microstructure in an Al Mg alloy during serrated flow. Mater Sci Eng A 1994;174:1 7.
[9] Robinson JM. Serrated flow in aluminium based alloys. Int Mater 1994;39:217 27.
[10] Louchet F. Flow stress anomalies, mobile dislocation exhaustion and strain rate sensitivity. Phil Mag 1995;72: 905 12.
[11] McCormick PG. Dynamic strain aging. Trans Ind Inst Met 1986;39:98 106.
[12] Rodriguez P. Serrated plastic flow. Bull Mater Sci 1984;6: 653 63.
[13] Chihab K, Estrin Y, Bubin LP, Vergnol J. The kinetics of the Portevin Le Châtelier bands in an Al 5Mg alloy. Scr Metall 1987;21:203 8.
[14] Kubin LP, Estrin Y. Evolution of dislocation densities and the critical conditions for the Portevin Lechâtelier effect. Acta Metall 1990;38:697 708.
[15] An YG, Wilson DV, Bate PS. The effect of strain path on the critical strain for serrated flow in solution treated AA6082. Scr Mater 1996;34:1641 6.
[16] Hayes JS, Keyte R, Plangnell PB. Effect of grain size on tensile behavior of a submicron grained Al 3Mg alloy produced by severe deformation. Mater Sci Tech 2000;16:1259 63.
[17] Muñoz Morris MA, Oca CG, Morris DG. Mechanical behavior of dilute Al Mg alloy processed by equal channel angular pressing. Scr Metall 2003;48:213 8.
[18] Markushev MV, Murashkin MY. Structure and mechanical properties of commercial Al Mg 1560 alloy after equal channel angular extrusion and annealing. Mater Sci Eng A 2004;367:234 42.
[19] Kapoor R, Gupta C, Sharma G, Chakravartty JK. Deformation behavior of Al 1.5Mg processed using the equal channel angular pressing technique. Scr Metall 2005;53:1389 93.
[20] Prados E, Sordi V, Ferrante M. Tensile behaviour of an Al 4Cu alloy deformed by equal channel angular pressing. Mater Sci Eng A 2009;503:68 70.
[21] Saha GG, McCormick PG, Rao PR. Portevin Le Châtelier effect in an Al Mn alloy II: yield transition and strain rate sensitivity measurements. Mater Sci Eng A 1984;62:187 96.
[22] Pink E. The effect of precipitation on characteristics of serrated flow in Al5Zn1Mg. Acta Metall 1989;37:1773 81.
[23] Kumar S, McShane HB. Serrated yielding in Al Li alloys. Scr Mater 1993;28:1149 54.
[24] Kumar S, Pink E. Serrated flow in aluminium alloys containing lithium. Acta Mater 1997;45:5295 301.
[25] Shen YZ, Oh KH, Lee DN. Serrated flow behavior in 2090 Al Li alloy influenced by texture and microstructure. Mater Sci Eng A 2006;435:343 54.
[26] Chmelík F, Pink E, Król J, Balík J, Pesicka J, Lukác P. Mechanisms of serrated flow in Al alloys with precipitates investigated by acoustic emission. Acta Mater 1998;46: 4435 42.
[27] Loannidis EK, Marshall GJ, Sheppard T. Microstructure and properties of extruded Al 6Mg 3Cr alloy prepared from rapidly solidified powder. Mater Sci Tech 1989;5:56 64.

[28] Abramov VO, Sommer F. Structure and mechanical \properties of rapidly solidified Al (Fe, Cr) and Al Mg (Fe, Cr) alloys. Mater Lett 1994;20:251 5.
[29] Maeng DY, Lee JH, Hong SI, Chun BS. Microstructure and mechanical properties of rapidly solidified Al 7wt.%Mg X (X=Cr, Zr or Mn) alloys. Mater Sci Eng A 2001;311:128 34.
[30] Shin DH. Superplastic behavior of rapidly solidified Al 5Mg 1.2Cr alloy. J Mater Sci Lett 1989;8:1412 3.
[31] Eddahbi M, Carsí M, Ruano OA. Characterization of a thermomechanically powder metallurgy Al 5Mg 1.2Cr alloy. Mater Sci Eng A 2003;361:36 44.
[32] Král R, Lukác P. Modelling of strain rate hardening and its relation to the onset of Portevin Le Châtelier effect in Al Mg alloy. Mater Sci Eng A 1997;234 236:786 9.
[33] Balík J, Lukác P, Kubin LP. Inverse critical strains for jerky flow in AlMg alloys. Scr Mater 2000;42:465 71.
[34] Eddahbi M, PhD dissertation, Facultad de Ciencias Físicas (1998). Universidad Complutense, Madrid.
[35] Kim IS, Chaturvedi MC. Serrated flow in Al 5wt.%Mg alloy. Mater Sci Eng A 1979;37:165 72.
[36] Roopchand BJ, Morris JG. The effect of cold work on the strain rate sensitivity of 5086 aluminium alloy. Scr Metall 1973;7: 839 46.
[37] Korbel A, Dybiec H. The problem of the negative strain rate sensitivity of metals under the Portevin Lechâtelier deformation conditions. Acta Metall 1981;29:89 93.
[38] Ait Amokhtar H, Boudrahem S, Fressengeas C. Spatiotemporal aspects of jerky flow in Al Mg alloys, in relation with the Mg content. Scr Mater 2006;54:2113 8.
[39] Thuillier S, Rauch EF. Interaction of microbands with grain boundaries in mild steel. Scr Mater 1995;32:541 6.